Smart Materials and Structures

ACCEPTED MANUSCRIPT

A Theoretical Analysis of Deformation Behavior of Auxetic Plied Yarn Structure

To cite this article before publication: jifang ZENG *et al* 2018 *Smart Mater. Struct.* in press https://doi.org/10.1088/1361-665X/aac23a

A Theoretical Analysis of Deformation Behavior of Auxetic Plied Yarn Structure

Jifang Zeng, Hong Hu*

Institute of Textile and Clothing, Hong Kong Polytechnic University, Hung Hom, Kowloon, Hong Kong, China

*Corresponding author

Tel: +852-3400 3089, Fax: +852-2773 1432

E-mail address: tchuhong@polyu.edu.hk

Abstract

This paper presents a theoretical analysis of the auxetic plied yarn (APY) structure formed with two types of single yarns having different diameter and modulus. A model which can be used to predict its deformation behavior under axial extension is developed based on the theoretical analysis. The developed model is first compared with the experimental data obtained in the previous study, and then used to predict the effects of different structural and material parameters on the auxetic behavior of the APY. The calculation results show that the developed model can correctly predict the variation trend of the auxetic behavior of the APY, which first increases and then decrease with the increase of the axial strain. The calculation results also indicate that the auxetic behavior of the APY simultaneously depends on the diameter ratio of the soft yarn and stiff yarn as well as the ratio between the pitch length and stiff yarn diameter. The study provides a way to design and fabricate APYs with the same auxetic behavior by using different soft and stiff yarns as long as these two ratios are kept unchanged.

Keywords

Auxetic yarn, negative Poisson's ratio, deformation behavior, geometrical analysis

Nomenclature

L – The length (pitch) of the auxetic plied yarn per one turn

L_0 – The value of L in the initial state

S_D – The length of the soft yarn per one turn

S_{D_0} – The value of S_D in the initial state

S_d – The length of the stiff yarn per one turn

S_{d_0} – The value of S_d in the initial state

D – The diameter of the soft yarn

D_0 – The value of D in the initial state

d – The diameter of the stiff yarn

d_0 – The value of d in the initial state

θ_D – The helical angle of the soft yarn

θ_{D_0} – The value of θ_D in the initial state

θ_d – The helical angle of the stiff yarn

θ_{d_0} – The value of θ_d in the initial state

y_D – The coordinate of the center of the soft yarn in *y* axis

y_{D_0} – The value of y_D in the initial state

x_d – The coordinate of the center of the stiff yarn in *x* axis

x_{d_0} – The value of x_d in the initial state

δ – The tilt angle of the stiff yarn

δ_0 – The value of δ in the initial state

γ – The tilt angle of the moving path of stiff yarn

H – The effective diameter of the auxetic plied yarn

H_0 – The value of H in the initial state

S – The distance between any point located on the outline of the soft yarn and the center of the auxetic plied yarn

ε – The axial strain of the auxetic plied yarn

ε_r – The radial strain of the plied yarn

ε_c – The critical axial strain of the auxetic plied yarn when the two stiff yarns get contacted each other

ν – The Poisson's ratio of the auxetic plied yarn

ν_D – The Poisson's ratio of the soft yarn

ν_d – The Poisson's ratio of the stiff yarn

Subscripts D and d – Indication of the soft yarn and stiff yarn, respectively

Subscript 0 – Indication of the initial state

1. Introduction

Auxetic materials deform in a different way from conventional materials. They laterally expand when stretched or laterally contract when compressed. This deformation behavior leads to the enhancement of a variety of their mechanical properties[1, 2], such as impact resistance[3], energy absorption[4, 5], resistance to fracture[6], and indentation resistance[7], etc. Since the first auxetic polymeric foam was produced by Lakes in 1987[8], investigations on auxetic materials[9-11], particularly on their fabrication[12-17] and characterization [18, 19], have become one of the hot research topics in material area. Meanwhile, a lot of auxetic structures[4, 8-11, 20-25] have been developed or proposed to make auxetic materials. As a special type of auxetic materials, auxetic yarns[13, 21, 24-28] play an important role as a base to fabricate auxetic textiles and composites.

Helical auxetic yarn (HAY)[19-21, 28-33] is the mostly reported auxetic yarn structure in auxetic textiles. It is formed with two single non-auxetic yarns in a helical arrangement. One is the core yarn and the other is the wrap yarn which is helically wound on the straight core yarn. When a HAY is subjected to an axial extension, its radial width will be increased due to the transversal displacement of the core yarn by the wrap yarn. Various studies have been done on HAY structure to identify key parameters to manipulate its auxetic behavior. The helical angle of the wrap yarn[19, 21, 30-33], Poisson's ratio[19, 33] and tensile modulus of the core and wrap yarns [28, 30-33], and the core yarn/wrap yarn diameter ratio[19, 21, 30-33] have been identified as the important parameters by experiments and finite element analyses. Among these parameters, the helical angle of the wrap yarn[19, 21, 30-33] has been found to have the most profound effect on auxetic behavior of HAY. The studies showed that the lower helical angle of the wrap yarn, the higher maximum auxetic effect of the HAY. A maximum negative Poisson's ratio of -12.04 could be achieved when the helical angle of the wrap yarn is lowered to 7^{o} according to McAfee's work[19]. By comparing the Poisson's ratio and extension strain relation of two HAYs made of core yarns with different Poisson's ratio (0.3 and 0.4), McAfee et al. [19] also found that the effect of the Poisson's ratio of the core yarn on the deformation behavior of the HAY could be negligible. On the other hand, Wright et al. [33] found that the auxetic effect of the HPY is increased from 0 to -0.45 with the decrease in the Poisson's ratio of both the core and wrap yarns. As for the effect of tensile modulus of the core yarn and wrap yarn, Bhattacharya et al.[28] found that the occurring of core-indentation effect depends on their relative modulus. Du et al.[31, 32] proved that the auxetic effect of HAY became more observable with higher tensile modulus of the wrap yarn. The same conclusion was also obtained by Wright et al.[33]. Investigations also showed that the core/wrap yarn diameter ratio has a significant effect on the auxetic behavior of HAY[19, 21,

30-33]. With decreasing the core/wrap yarn diameter ratio, the auxetic effect of HAY became less visible. In addition to the quasi-static tensile test, Zhang et al.[29] also investigated the dynamic thermo-mechanical and impact properties of HAY. They found that the dynamic thermo-mechanical properties are significantly affected by the core/wrap diameter ratio and the initial wrap angle[29]. It should be noted that although the helical angle of the wrap yarn[19, 21, 31-33] has significant effect on the auxetic behavior of HAY, it is very difficult to maintain the same helical angle throughout the whole HAY, because the slippage of the wrap yarn occurs easily on the surface of the core yarn[20, 25]. Meanwhile, the uneven state is usually arrived after the extension. To solve these problems, the HAY was enclosed by an appropriate layer of sheath to maintain its auxetic behavior[20]. This improvement did not only facilitate the fabrication, but also enlarged the application of HAYs.

Inspired from the HAY, Ge et al.[25] proposed another type of auxetic yarn called auxetic plied yarn (APY). Different from HAY, APY is formed with two types of single yarns having different moduli and diameters to improve auxetic yarn structural stabilization. In an APY structure, two stiff yarns with a relatively high modulus and two soft yarns with a relatively small modulus are alternately arranged and twisted together in a helical way. Due to the significant difference in the yarn modulus between the soft and stiff yarns, the stiff yarns tend to move towards the center of the APY and push the soft yarns outwards under the axial extension. As a result of this deformation mechanism, the auxetic behavior is achieved in the APY structure. Ge et al. first experimentally investigated the auxetic behavior of the APYs[25]. According to their experimental results, the auxetic behavior of the APYs rapidly increases in the initial stage of the axial extension and then gradually decreases with further increase of the axial strain. This variation trend was then confirmed by Ng and Hu based on both tensile test and cross sectional analysis[34]. In order to predict the auxetic behavior of

the APY structure, Ge et al. also conducted a geometrical analysis[25]. In their analysis, the deformation process of the APY is divided into two stages by a critical state where the two stiff yarns just get contacted each other at the center of the APY structure. The axial extension strain at this state is defined as a critical strain. Although their geometrical analysis could well predict the auxetic behavior of the APY structure in high axial strain range, the difference in the initial extension stage is very high. Especially, the variation trends of the auxetic behavior between the experiment and prediction are opposite. While the experimental results show that the auxetic behavior of the APY increases at the initial stage of extension, the predicting results demonstrate the auxetic behavior decreases, making the deformation behavior of the APY structure unclear.

In order to better understand the deformation behavior of the APY structure and to precisely predict its Poisson's ratio especially in the initial extension stage, a new theoretical analysis is presented in this paper. The model obtained from the analysis is firstly validated with the experimental results from reference [34], and then used to predict the effects of different structural parameters. It is expected that the outcomes of this study could provide a better understanding of the deformation behavior of APY structure.

2. Theoretical analysis

2.1 APY structure and assumptions

The 3D view of an APY structure is shown in Fig.1a. It is formed by twisting two soft yarns and two stiff yarns together into a helical shape. Depending on the diameter ratio between the soft yarn and stiff yarn as well as the initial twisting value, three possible structures can be obtained and their cross sections in an ideal initial state are shown in Fig.1b-d, respectively. As explained before, because of the difference in the yarn modulus, the stiff yarns tend to move toward the center of the APY and push the soft yarn outward under the axial extension

until the two stiff yarns get contacted each other. After this state, both the stiff and soft yarns start to contract to the center of the APY with further axial extension. Hence, the structures shown in Fig.1b and 1c will perform auxetic behavior as a result of the increase of the effective diameter of the APY when stretched. Differently, a non-auxetic behavior is achieved by the structure shown in Fig.1d in the initial stage of the axial extension because the effective diameter of APY will be reduced when the stiff yarns start to move towards the APY center. Due to this reason, only structures shown in Fig. 1b and 1c are considered in this analysis. In this case, the effective diameter of the APY is determined by the profile of the soft yarns accordingly.

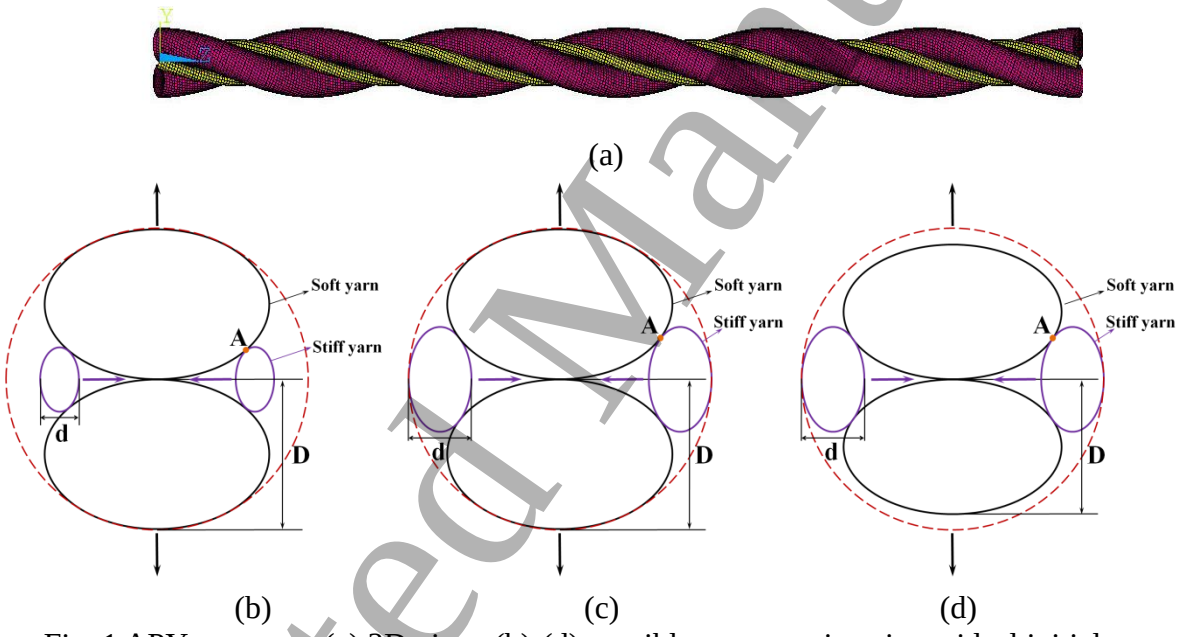

Fig. 1 APY structure: (a) 3D view; (b)-(d) possible cross sections in an ideal initial state

To facilitate the analysis, the following assumptions are first made. Meanwhile, all symbols used during the analysis are listed in Nomenclature for easy check and reference.

1) All the single yarn components are transversal isotropic linear elastic materials with known Poisson's ratio values and their cross sections are circular and are kept circular when extended in their axial direction.

2) The extrusion and friction among the yarn components during the axial extension process are ignored in the theoretical analysis.

3) The APY is twisted uniformly so that only one turn is sufficient to characterize its deformation behavior under axial extension.

4) In the initial state, the two soft yarns closely contact at the central point of the APY. However, due to untwisting trend of the yarns in the relaxed state, the centers of the two stiff yarns are deviated from x axis as shown in Fig. 2a. In this case, the two stiff yarns cannot keep symmetrical contacts with the two soft yarns. Instead, each stiff yarn has only a contact with a soft yarn and a tilt angle δ_0 will be used to define the initial position of each stiff yarn.

5) The deformation process of the APY can be divided into two stages. The first stage is defined from the initial state to the state where the two stiff yarns fully move towards the center of the APY structure and just get in contact each other, as shown in Fig. 2b. This state is called critical state and the axial extension strain at this state is defined as a critical strain. Different from the previous analysis[25], in the first stage shown in Fig.2c, each stiff yarn is assumed to move towards the center of the APY with a constant tilt angle γ as shown Fig. 2d. As the stiff yarns are difficult to be extended under low loading condition, their diameter and length are assumed to be kept constant in this stage. However, the diameter and length of the soft yarns can be changed due to lower modulus. The second stage is defined from the critical state to the failure of the APY structure. As shown in Fig. 2e, the main deformation mode in the second stage is the cross sectional contraction of all the yarn components due to high extension. Besides, the diameter and length of the stiff yarns are no longer assumed to be constant.

Based on the above assumptions, the theoretical analysis will be carried for the APY structure

in the different states and deformation stages.

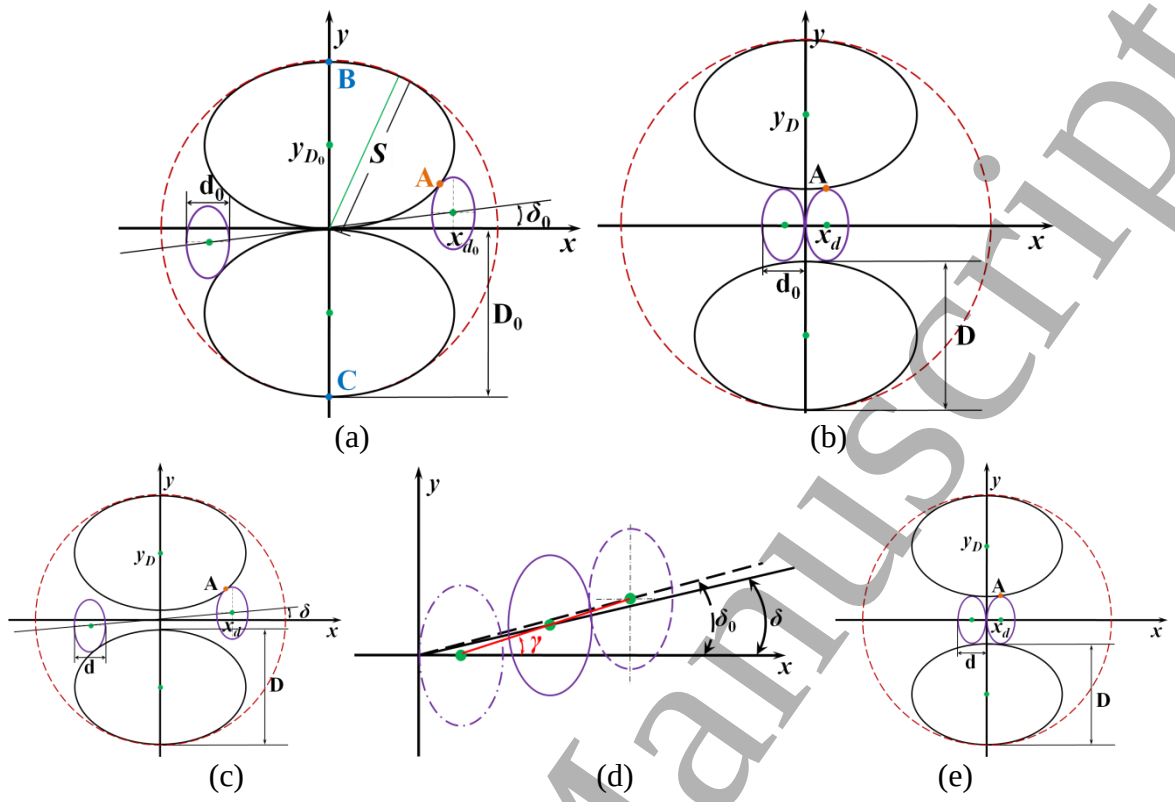

Fig. 2 APY in the different states: (a) the initial state; (b) the critical state where the two stiff yarns just get contact; (c) any state in the first stage; (d) the moving path of the stiff yarn in the first stage; (e) any state in the second stage.

2.2 The initial state

According to Assumption 4, in the initial state, each stiff yarn has only a contact with a soft yarn. As shown in Fig. 2a, tilt angle δ_0 defines the initial position of each stiff yarn. As the cross sections of both the soft yarn and stiff yarn are assumed to be circular, their outlines on the cross section of the APY are in elliptical forms. For the soft yarns, the short axes and long axes of their cross sections are parallel to *y* axis and *x* axis, respectively. For the stiff yarns, as their centers are deviated from *x* axis, their short and long axes are no longer parallel to *x* axis and *y* axis. However, as the deviation is very small, their short and long axes are still assumed to be parallel to *x* axis and *y* axis for facilitating the analysis. By considering the symmetrical feature of the APY cross sectional structure, only the right stiff yarn and upper soft yarn are

selected for the analysis and the outlines of their cross sections can be described by Eq. 1 and Eq. 2, respectively, when the coordinate origin is set at the center of the APY.

$$\left(x - x_{d_0}\right)^2 + \left(y_{\text{stiff}} - x_{d_0}\tan\delta_0\right)^2 \cos^2\theta_{d_0} = \frac{d_0^2}{4} \tag{1}$$

$$x^2\cos^2\theta_{D_0} + \left(y_{\text{soft}} - y_{D_0}\right)^2 = \frac{D_0^2}{4} \tag{2}$$

Here, y_{stiff} and y_{soft} are used to identify the two types of yarns. As the two soft yarns are assumed to contact each other in the initial state, Eq. 3 is obtained.

$$y_{D_0} = \frac{D_0}{2} \tag{3}$$

Fig. 3a shows the side view of the APY in the initial state. Its helical form can be expanded by untwisting. Fig. 3b shows both the soft yarn and stiff yarn after the spiral expansion. From Fig. 3b, Eq. 4 to Eq. 6 can be obtained.

$$\cos\theta_{d_0} = \frac{L_0}{S_{d_0}} \tag{4}$$

$$\cos\theta_{D_0} = \frac{L_0}{S_{D_0}} = \frac{L_0}{\sqrt{L_0^2 + \pi^2 D_0^2}} \tag{5}$$

$$x_{d_0} = \frac{\sqrt{S_{d_0}^2 - L_0^2}}{2\pi}\cos\delta_0 \tag{6}$$

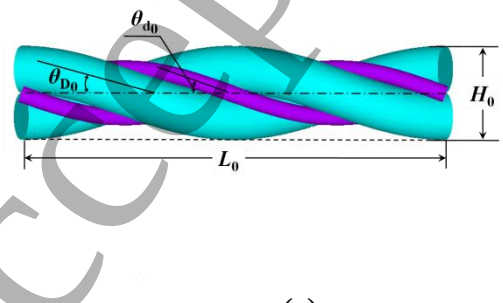

(a)

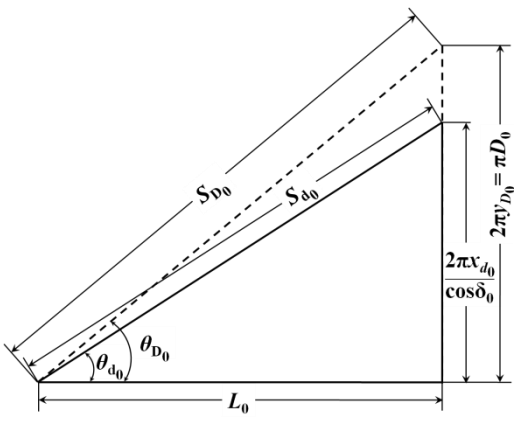

(b)

Fig. 3 APY in the initial state: (a) the side view; (b) after spiral expansion.

By substituting Eq. 4 and Eq. 6 into Eq. 1, and Eq. 3 and Eq. 5 into Eq. 2, Eq. 7 and Eq. 8 are obtained.

$$y_{\text{stiff}} = \frac{S_{d_0}\sqrt{\frac{d_0^2}{4} - \left(x - \frac{\sqrt{S_{d_0}^2 - L_0^2}}{2\pi}\cos\delta_0\right)^2}}{L_0} + \frac{\sin\delta_0\sqrt{S_{d_0}^2 - L_0^2}}{2\pi} \tag{7}$$

$$y_{\text{soft}} = \frac{D_0}{2} - \sqrt{\frac{D_0^2}{4} - \frac{L_0^2}{L_0^2 + \pi^2 D_0^2}x^2} \tag{8}$$

In the initial state, structural parameters D_0, d_0, L_0 and S_{d_0} can be directly measured. These parameters determine the geometry of the APY. By giving the values of these parameters, the value of δ_0 can be found from Eq. 7 and Eq. 8 by applying an approximation method which is called binary search. The way is to search the contact point A(x_A, y_A) between the stiff yarn and soft yarn by calculating all values of y_{soft} and y_{stiff} when x is changed from $x_{d_0} - d_0/2$ to x_{d_0} as A falls in this interval. If for a given δ_0, the minimal value of the difference minΔy among all $\Delta y = y_{\text{soft}} - y_{\text{stiff}}$ is found between 0 and ξ, where ξ is the calculation accuracy and its value is selected as 10^{-5} in this study, it means that the stiff yarn just gets close enough to be contacted with the soft yarn at point A and the given value of δ_0 is the solution. If 0≤ minΔy≤ ξ cannot be met, change the value of δ_0 to recalculate all values of Δy again. In a general way, the initial value of δ_0 can be set at 45°. In this situation, the calculation process is given as follows.

a) Let δ_0=45°, calculate all Δy when x is changed from $x_{d_0} - d_0/2$ to x_{d_0}.

b) If the minΔy <0, it means that the stiff yarn is overlapped with the soft yarn, then set $\delta_0 = \delta_0/2$ to move the stiff yarn down away from the soft yarn; if minΔy > ξ, it means that

the stiff yarn keeps away from the soft yarn, then set $\delta_0 = (\delta_0 + 90)/2$ to move the stiff yarn up close to the soft yarn. In both cases, recalculate all Δy again when x is changed from $x_{d_0} - d_0/2$ to x_{d_0}.

c) Repeat process b) until $0 \leqslant \min\Delta y \leqslant \xi$ is found. When this condition is met, it means that the stiff yarn and contact yarn get close enough to be considered as contacted, and then δ_0 is the solution.

In the practical calculation, as the tilt angle δ_0 is very small in a real APY, the initial value of δ_0 is not necessary to set at 45°. In this study, the range of δ_0 is set from 0° to 10° to accelerate the calculation process. In addition, this approximation method can be also used in Ge's model[25] to calculate the helical angle of the soft yarn at a given axial tensile strain. In this way, the solution for a set of nonlinear equations including trigonometric functions and power functions is replaced by a simple binary search. Thus, the calculation is greatly simplified.

After δ_0 is known, the location of the center of the stiff yarn can be calculated from Eq. 6. Then the geometry of the APY in the initial state can be determined.

2.3 The first stage of deformation

According to Assumption 5, the first stage of the deformation of the APY structure under axial extension is defined from the initial state to the critical state where the two stiff yarns just get contacted each other at the center of the APY. As shown in Fig. 2d, in the first stage, the stiff yarn moves towards the center of the APY along a constant tilt angle γ. Considering an arbitral state at an axial strain ε, the pitch length of the APY is changed to L, which is given by Eq.9.

$$L = L_0(1+\varepsilon) \tag{9}$$

In the first stage, the diameter and length are kept unchanged according to Assumption 5. Therefore, we have $d = d_0$ and $S_d = S_{d_0}$. Similar to the initial state, the equations to describe the outlines of the cross-sections of the stiff and soft yarns can be derived from their elliptical shapes and are given by Eq. 10 and Eq. 11, respectively.

$$\left(x - x_d\right)^2 + \left(y_{\text{stiff}} - x_d \tan\delta\right)^2 \cos^2\theta_d = \frac{d_0^2}{4} \tag{10}$$

$$x^2 \cos^2\theta_D + \left(y_{\text{soft}} - y_D\right)^2 = \frac{D^2}{4} \tag{11}$$

As shown in Fig.4b, the following equations can be obtained from the spiral expansion of the stiff yarn and soft yarn.

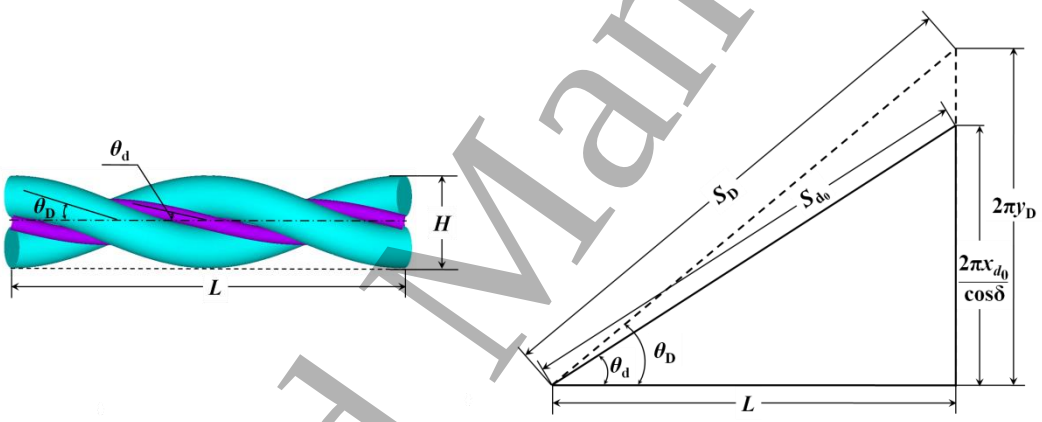

(a) (b)

Fig. 4 APY in the first stage: (a) the side view; (b) after spiral expansion.

$$y_D = \frac{L\tan\theta_D}{2\pi} \tag{12}$$

$$S_D = \frac{L}{\cos\theta_D} = L\sqrt{1+\tan^2\theta_D} \tag{13}$$

$$x_d = \frac{\sqrt{S_{d_0}^2 - L^2}\cos\delta}{2\pi} \tag{14}$$

$$S_d = S_{d_0} = \frac{L}{\cos\theta_d} = L\sqrt{1+\tan^2\theta_d} \tag{15}$$

In the first stage, ε is changed from 0 to ε_c where ε_c is the axial strain at the critical state. For

a given axial strain ε, the variable θ_d can be calculated from Eq.9 and Eq.15 together. It should be noted that δ is not constant. Its relations with δ_0 and γ can be determined according to the moving path of the stiff yarn as shown in Fig.2d. From Figure, Eq.16 and Eq. 17 can be obtained.

$$\frac{\tan\gamma}{\tan\delta_0} = \frac{x_{d_0}}{x_{d_0} - d_0/2} \tag{16}$$

$$\frac{\tan\gamma}{\tan\delta} = \frac{x_d}{x_d - d_0/2} \tag{17}$$

Substituting Eq.6 into Eq.16, and Eq.14 into Eq.17, Eq. 18 and Eq.19 are obtained.

$$\tan\gamma = \frac{\sqrt{S_{d_0}^2 - L_0^2}\sin\delta_0}{\sqrt{S_{d_0}^2 - L_0^2}\cos\delta_0 - \pi d_0} \tag{18}$$

$$\tan\gamma = \frac{\sqrt{S_{d_0}^2 - L^2}\sin\delta}{\sqrt{S_{d_0}^2 - L^2}\cos\delta - \pi d_0} \tag{19}$$

From Eq. 18 and Eq. 19, Eq. 20 is obtained.

$$\cos\delta = \frac{\dfrac{\tan^2\gamma\pi d_0}{\sqrt{S_{d_0}^2 - L^2}} \pm \sqrt{\left(\tan^2\gamma + 1\right) - \dfrac{\tan^2\gamma\pi^2 d_0^2}{S_{d_0}^2 - L^2}}}{\tan^2\gamma + 1} \tag{20}$$

Thus, δ can be calculated from Eq. 18 and Eq. 20 together. When δ is known, x_d can be calculated from Eq.14. According to Assumption 1, the diameter of the soft yarn D in the stretched state can be calculated by Eq. 21.

$$D = D_0\left(1 - \frac{S_D - S_{D_0}}{S_{D_0}}\nu_D\right) \tag{21}$$

Substituting Eq.9 and Eq.13 into Eq.21, Eq. 22 is obtained

$$D = \left[1 + \nu_D - (1+\varepsilon)\nu_D \frac{\cos\theta_{D_0}}{\cos\theta_D} \right] D_0 \tag{22}$$

Where $\cos\theta_{D_0}$ is given by Eq. 5.

By firstly substituting Eq. 9, Eq. 14 and Eq. 15 into Eq.10, then Eq. 12 and Eq.22 into Eq. 11, Eq. 23 and Eq. 24 can be obtained. By using the same binary search method as presented above, the helical angle θ_D of the soft yarn for a given axial strain ε can be found based on the comparison of y_{soft} and y_{stiff}. When θ_D is known, y_D and D can be calculated from Eq. 12 and Eq. 22, respectively. Then the geometry of the APY in the first stage for a given ε between 0 and ε_c can be determined.

$$y_{\text{stiff}} = \frac{\sqrt{S_{d_0}^2 - L_0^2(1+\varepsilon)^2}\sin\delta}{2\pi} + \sqrt{\frac{d_0^2}{4} - \left(x - \frac{\sqrt{S_{d_0}^2 - L_0^2(1+\varepsilon)^2}\cos\delta}{2\pi} \right)^2} \frac{S_{d_0}}{L_0(1+\varepsilon)} \tag{23}$$

$$y_{\text{soft}} = \frac{L_0(1+\varepsilon)\tan\theta_D}{2\pi} - \sqrt{\frac{\left[1 + \nu_D - \dfrac{(1+\varepsilon)\nu_D L_0}{\cos\theta_D \sqrt{L_0^2 + \pi^2 D_0^2}} \right]^2 D_0^2}{4} - x^2\cos^2\theta_D} \tag{24}$$

2.4 The critical state

The critical state is defined when the two stiff yarns just get contacted each other according to Assumption 5. As shown in Fig. 2b, in the critical state, $x_d = d_0/2$ and $S_d = S_{d_0}$. From these conditions, the axial critical strain ε_c can be calculated. The spiral expansion of the stiff yarn gives Eq. 25.

$$S_{d_0}^2 = L_0^2(1+\varepsilon_c)^2 + (\pi d_0)^2 \tag{25}$$

From Eq. 25, ε_c can be derived and is given by Eq. 26.

$$\varepsilon_c = \frac{S_{d_0}\cos\theta_d}{L_0} - 1 = \frac{\sqrt{S_{d_0}^2 - \pi^2 d_0^2}}{L_0} - 1 \tag{26}$$

2.5 The second stage of deformation

The second stage is defined from the critical state to the failure of the APY. In this stage, the stiff yarns always keep contact together at the center of the APY and their diameter and length are no longer assumed to be constant. According to Assumption 1 and 5, Eq. 27 and Eq. 28 can be obtained.

$$x_d = d/2 \tag{27}$$

$$d = d_0\left(1-\frac{S_d - S_{d_0}}{S_{d_0}}\nu_d\right) \tag{28}$$

In the second stage, the equations for the outlines of the stiff and soft yarns are given by Eq. 29 and Eq. 30.

$$\left(x-\frac{d}{2}\right)^2 + y_{\text{stiff}}^2\cos^2\theta_d = \frac{d^2}{4} \tag{29}$$

$$x^2\cos^2\theta_D + \left(y_{\text{soft}} - y_D\right)^2 = \frac{D^2}{4} \tag{30}$$

As shown in Fig.5b, the following equations can be obtained from the spiral expansion of the stiff yarn and soft yarn.

$$\cos\theta_d = \frac{L}{S_d} \tag{31}$$

$$S_d^2 = (1+\varepsilon)^2 L_0^2 + \pi^2 d^2 \tag{32}$$

$$S_D = \frac{L}{\cos\theta_D} \tag{33}$$

$$y_D = \frac{L\tan\theta_D}{2\pi} \tag{34}$$

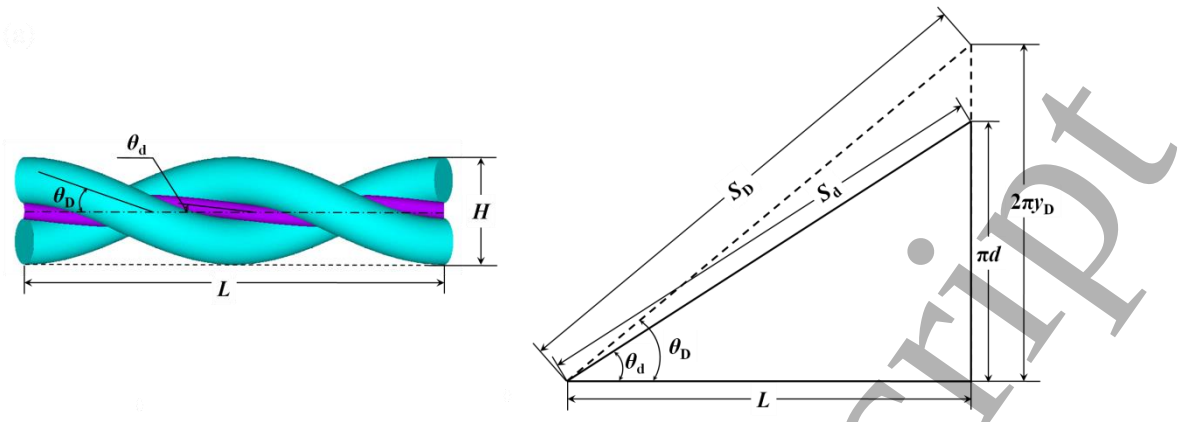

(a) (b)

Fig. 5 APY in the second stage: (a) the side view; (b) after spiral expansion.

Substituting Eq.28 into Eq.32, Eq.35 is obtained

$$\left(\frac{\pi^2}{S_{d_0}^2}-\frac{1}{\nu_d^2 d_0^2}\right)d^2+\frac{2}{\nu_d d_0}\left(\frac{1}{\nu_d}+1\right)d+\frac{L_0^2(1+\varepsilon)^2}{S_{d_0}^2}-\left(\frac{1}{\nu_d}+1\right)^2=0 \qquad (35)$$

By solving Eq. 35, the diameter of the stiff yarn in the second stage d is obtained and given by Eq. 36.

$$d=\frac{-\frac{1}{\nu_d d_0}\left(\frac{1}{\nu_d}+1\right)+\sqrt{\frac{L_0^2(1+\varepsilon)^2}{\nu_d^2 d_0^2 S_{d_0}^2}-\frac{\pi^2}{S_{d_0}^2}\left(\frac{L_0^2(1+\varepsilon)^2}{S_{d_0}^2}-\left(\frac{1}{\nu_d}+1\right)^2\right)}}{\frac{\pi^2}{S_{d_0}^2}-\frac{1}{\nu_d^2 d_0^2}} \qquad (36)$$

When d is known for a given ε, the length and helical angle of the stiff yarn can be obtained by Eq.32 and Eq.31, respectively. In addition, the value of x_d is also determined from Eq.27. Hence, all variables for stiff yarn have been obtained. For the soft yarn, its diameter can be determined by the same Eq. 22 derived in the first stage. By substituting Eq.5 into Eq. 22, Eq. 37 is obtained.

$$D=D_0\left(1-\frac{\frac{L_0(1+\varepsilon)}{\cos\theta_D}-\sqrt{L_0^2+\pi^2 D_0^2}}{\sqrt{L_0^2+\pi^2 D_0^2}}\nu_D\right) \qquad (37)$$

By substituting Eq.31 and Eq.32 into Eq.29, substituting the Eq.9 and Eq.34 into Eq.30, Eq.38 and Eq.39 are obtained

$$y_{\text{stiff}} = \frac{\sqrt{(1+\varepsilon)^2 L_0^2 + \pi^2 d^2}}{L_0(1+\varepsilon)} \sqrt{xd - x^2} \tag{38}$$

$$y_{\text{soft}} = \frac{L_0(1+\varepsilon)\tan\theta_D}{2\pi} - \sqrt{\frac{D^2}{4} - x^2\cos^2\theta_D} \tag{39}$$

Where, d and D are given by Eq.36 and Eq.37. By using the same binary search method as presented above, the helical angle θ_D of the soft yarn for a given axial strain ε can be found based on the comparison of y_{soft} and y_{stiff} calculated from Eq. 39 and Eq. 38, respectively. When θ_D is known, y_D and D can be calculated from Eq. 34 and Eq. 37, respectively. Then the geometry of the APY in the second stage for a given $\varepsilon > \varepsilon_c$ can be determined.

2.6 Determination of effective diameter of the APY

The objective of this study is to theoretically calculate the Poisson's ratio of the APY for the initially given structural parameters D_0, d_0, L_0, and S_{d_0}. At a given axial strain ε, the Poisson's ratio of the APY v can be calculated from Eq. 40.

$$v = -\frac{\varepsilon_r}{\varepsilon} = -\frac{H - H_0}{H_0} / \varepsilon = \left(1 - \frac{H}{H_0}\right) / \varepsilon \tag{40}$$

Eq.40 indicates that the calculation of v needs to first know the effective diameter in the initial state H_0 and the effective diameter in the stretched state H. The following analysis shows how to determine H_0 and H based on the above analysis.

As mentioned before, only the APY structures shown in Fig. 1b and 1c are considered in this analysis. Therefore, only points on the outlines of the two soft yarns are used to determine the effective diameter of the APY. It should be pointed out that as the outlines of the soft yarns in the cross section of the APY have an elliptical form, the distance between the two short axis

extremities of the soft yarns BC may not be the effective diameter of the APY, as shown in Fig. 2a. Therefore, the maximal distance between two points on the outlines of the soft yarns should be determined as the effective diameter of the APY.

Let us first determine H_0 in the initial state. As shown in Fig. 2a, the distance S between an arbitrarily point (x,y) located on the outline of the soft yarn and the center (0,0) of the APY can be described by Eq.41. Obviously, the maximal value of this distance S_{max} is the effective radius of the APY.

$$S^2 = x^2 + y^2 \tag{41}$$

By eliminating x with the use of Eq. 2, Eq. 41 becomes Eq. 42.

$$S^2 = \frac{\frac{D_0^2}{4} - \left(y - y_{D_0}\right)^2}{\cos^2\theta_{D_0}} + y^2 = \frac{-y^2\sin^2\theta_{D_0} + 2y_{D_0}y + \frac{D_0^2}{4} - y_{D_0}^2}{\cos^2\theta_{D_0}} \tag{42}$$

Because the distance S is positive, S and its square S^2 will have the same point of y for their maximal values S_{max} and S_{max}^2. For this reason, Eq. 42 is adopted to determine the maximal point of y for calculating S_{max}. The process includes the following steps.

Step 1: Define the interval of y. As shown in Fig. 2a, the defined interval of y for calculating S_{max} is $y_{D_0} \leqslant y \leqslant y_{D_0} + D_0/2$, including the two end points of the interval y_{D_0} and $y_{D_0} + D_0/2$.

Step 2: Determine the extreme point y_0 for calculating S_{max}. To do that, the first and second derivatives of S^2 are derived as shown in Eq. 43. The value of y_0 is obtained when $\left(S^2\right)' = 0$. Its solution is given by Eq. 44. Because $\left(S^2\right)''$ is negative, S^2 is a convex function. Hence, S is a convex function too. Therefore, the value of S calculated when $y = y_0$ is its maximal value.

$$\left(S^2\right)' = 2\left(1-\frac{1}{\cos^2\theta_{D_0}}\right)y + \frac{2y_{D_0}}{\cos^2\theta_{D_0}} = \frac{2}{\cos^2\theta_{D_0}}\left(y_{D_0} - y\sin^2\theta_{D_0}\right) \tag{43}$$

$$\left(S^2\right)'' = -2\tan^2\theta_{D_0} < 0,$$

$$y_0 = \frac{y_{D_0}}{\sin^2\theta_{D_0}} \tag{44}$$

Step 3: Check whether y_0 falls in the defined interval. From Eq. 44, it is found that $y_0 > y_{D_0}$. Hence, y_0 should be compared with another end point $y_{D_0} + D_0/2$. To do that, Eq. 45 is introduced.

$$\Delta = \frac{y_{D_0}}{\sin^2\theta_{D_0}} - \left(y_{D_0} + \frac{D_0}{2}\right) = \frac{y_{D_0}}{\tan^2\theta_{D_0}} - \frac{D_0}{2} \tag{45}$$

From Fig. 3b, we can find Eq. 46.

$$y_{D_0} = \frac{L_0\tan\theta_{D_0}}{2\pi} \tag{46}$$

By substituting Eq. 46 into Eq. 45, we can obtain Eq. 47.

$$\Delta = \frac{L_0}{2\pi\tan\theta_{D_0}} - \frac{D_0}{2} \tag{47}$$

If $\Delta < 0$, it means that y_0 falls in the interval $y_{D_0} \le y \le y_{D_0} + D_0/2$. In this case, $S_{\max}$ is calculated when $y = y_0 = y_{D_0}/\sin^2\theta_{D_0}$. $\Delta < 0$ also means $L_0 - D_0\pi\tan\theta_{D_0} < 0$. If $\Delta \geqslant 0$, it means that y_0 falls out of the interval $y_{D_0} \le y \le y_{D_0} + D_0/2$ or just on the end point $y_{D_0} + D_0/2$. In this condition, $S_{\max}$ is calculated when $y = y_{D_0} + D_0/2$. $\Delta \geqslant 0$ also means $L_0 - D_0\pi\tan\theta_{D_0} \ge 0$.

By considering the above two cases, the maximum value of S can be calculated from Eq. 48.

$$S_{\max}=\begin{cases} S\big|_{y=y_{D_0}+\frac{D_0}{2}}=\dfrac{L_0\tan\theta_{D_0}}{2\pi}+\dfrac{D_0}{2}=D_0, & \left(L_0-\pi D_0\tan\theta_{D_0}\geq 0\right) \\ S\big|_{y=\frac{y_{D_0}}{\sin^2\theta_{D_0}}}=\dfrac{\sqrt{L_0^2+\pi^2D_0^2}}{2\pi\cos\theta_{D_0}}, & \left(L_0-\pi D_0\tan\theta_{D_0}<0\right) \end{cases} \tag{48}$$

From here, the effective diameter of the APY in the initial state can be determined as

$$H_0=2S_{\max} \tag{49}$$

The same way can be used to determine the effective diameter H in the first and second stage of deformation as given by Eq.50. In the previous study[25], the effective diameter was obtained by comparing among the distances calculated from all the points located on the outlines of both the stiff and soft yarns. This method is not only very time-consuming; the accuracy also completely depends on the numbers of the calculated distances. But in the present study, the effective diameter of the APY can be directly obtained from Eq.48 and Eq.50 after a simple judgment. The new method not only simplifies the calculation process and saves the time, the accuracy is also enhanced.

$$H=2S_{\max}=\begin{cases} 2S\big|_{y=y_D+\frac{D}{2}}=\dfrac{L\tan\theta_D}{\pi}+D, & \left(L-\pi D\tan\theta_D\geq 0\right) \\ 2S\big|_{y=\frac{y_D}{\sin^2\theta_D}}=\dfrac{\sqrt{L^2+\pi^2D^2}}{\pi\cos\theta_D}, & \left(L-\pi D\tan\theta_D<0\right) \end{cases} \tag{50}$$

Based on the above analysis, the whole calculating procedure of the Poisson's ratio v is finally summarized in Fig. 6. By giving the initial structural parameter of the APY D_0, d_0, L_0 and S_{d_0}, v can be calculated for any given axial strain ε.

3. Comparison with experiment

Before investigating the effects of structural parameters on the auxetic behavior, the theoretical analysis is firstly compared with the experiment. As this study only focuses on the theoretical analysis, the experimental data obtained by Ng et al. in their work[34] are used for

comparison. In this case, the initial structural parameters of the APY are set to be the same as obtained in [34] and relisted in Table1. In addition to these initial parameters, the Poisson's ratios of both the soft yarn ν_D and stiff yarn ν_d are also required for calculation. Their values are assumed to be the same and equals to 0.15, that is, $\nu_d = \nu_D = 0.15$. With these given values in the initial state, the initial tilt angle δ_0 is first calculated and its value obtained is 2.910°. Due to the introduction of δ_0, the term "tilted angle model" is used to indicate the present analysis in the following discussion.

Table 1 The geometrical parameters in the initial state used for calculation[34]

APY	Soft yarn	Stiff yarn	
Length L_0 (mm)	Diameter D_0 (mm)	Diameter d_0 (mm)	Length S_{d_0} (mm)
19.60	2.18	0.77	20.82

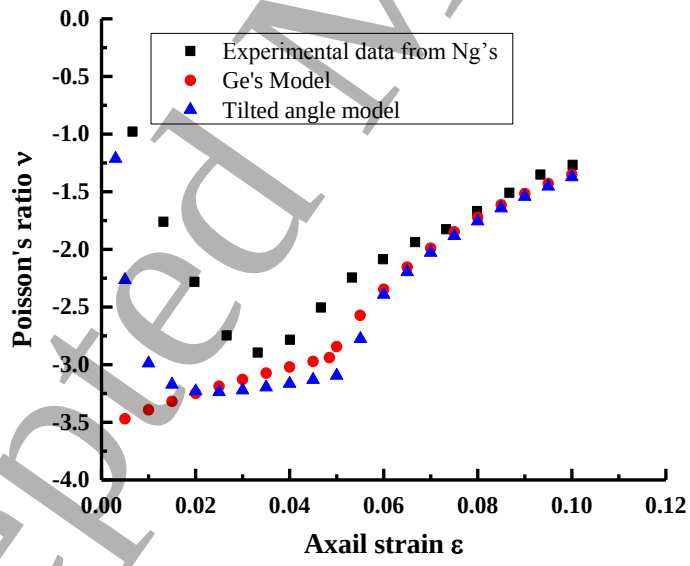

Fig. 7 Poisson's ratio as a function of axial strain obtained from experiment and theoretical claculation.

The Poisson's ratio values as a function of axial strain obatined from the experiment and

theoretical calculation are shown in Fig.7. For the comparison, the theoretical results calculated based on the Ge's model[25] without considering the initial tilt angle δ_0 are also shown in Fig.7. In fact, the Ge's model is a scpecial case of the present study when δ_0 = 0. From Fig.7, it can be seen that the tilted angle model gives a better prediction of the Poisson's ratio of the APY than the Ge's model as the Poisson's ratio calculated by the tilted angle model has the same variation trend as that of the experimental results, especially in the initial deformation stage when the axial tension strain is less than 0.04. This means that the introduction of the initial tilt angle δ_0 can improve the prediction of the deformation behavior of the APY in the initial stage, although the Poisson's ratio predicted by Ge's model is a little bit better than the tilted angle model for the axial strain between 0.02 and 0.07. The constant angle of moving path for the stiff yarn in first stage is a possible reason to cause this discrepancy. However, the auxetic behavior of the APY obtained from the titled angle model is still higher than that obtained from the experiment. There are several reasons to explain this difference. The first possible reason is the assumption for the constant diameter and length of the stiff yarn in the first stage of deformation. In fact, the stiff yarn gets slightly thinner and longer even in the lower axial strain. The second possible reason is the assumption for the ignorance of extrusion and friction among yarn components during the axial extension process. Actually, the friction among the yarns takes place in the first stage of the deformation due to the moving of the two stiff yarns towards the center of the APY. In addition, the indentation effect also occurs under the compression loads between the yarns. The other possible reasons include the uneven yarn twist and yarn cross section shapes. These reasons lead to an overestimation of the equivalent diameter of the APY in the theoretical calculation. However, with the increase of the axial strain, the difference in the Poisson's ratio between the theoretical calculation and experiment decreases. Although the difference exists in the initial

stage of the extension, the tilted angle model can well predict the variation trend of the Poisson's ratio, which helps better under understand the auxetic behavior of the APY. Therefore, this model is used to predict the effects of different structural and material parameters on the auxetic behavior of the APY.

4. Effects of structural and material parameters

The most important point of the present analysis is the introduction of the initial tilt angle of the stiff yarn δ_0. Thus, the effect of δ_0 on the auxetic behavior of the APY is firstly discussed here. As $\delta_0$is determined by the initial length S_{d_0}, changing of $\delta_0$means changing of S_{d_0}. Fig. 8 shows the calculation results with different values of δ_0 when other structural parameters listed in Table 1 are kept unchanged except S_{d_0}. It can be seen that the effect of δ_0 is very small, especially nearly negligible when the axial strain is larger than 0.5. Therefore, δ_0 will be kept constant when discussing the effects of other parameters. For consistency with the above calculation, the value of δ_0 is kept as δ_0 =2.910 °.

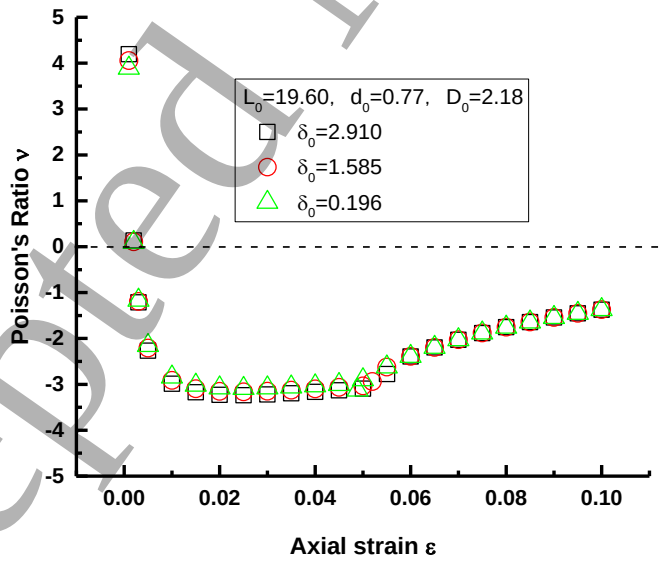

Fig. 8 Effect of δ_0 on auxetic behavior of APY

The second parameter is the value of the Poisson's ratio of the soft yarn and soft yarn. Fig. 9

shows the calculation results with two Poisson's ratio values of the soft and stiff yarns. It can be found that there is almost no effect of the Poisson's ratio of the soft and stiff yarns on the auxetic behahior of the APY before the axial strain reaches the critical strain ε_c. Although the effect of the Poisson's ratio of the yarns can be noted after ε_c, the effect is very small. After ε_c, the auxetic behavior of APY is slightly decreased with the increase of the Poisson's ratio of the soft and stiff yarns. This decrease in the auxetic effect of the APY is mainly caused by the reduction of the diameter of the soft and stiff yarns in the high axial strain. Since the effect of the Poisson's ratio of the soft and stiff yarns is very small, its value is kept unchanged when discussing the effects of other parameters, that is, $\nu_d=\nu_D=0.15$.

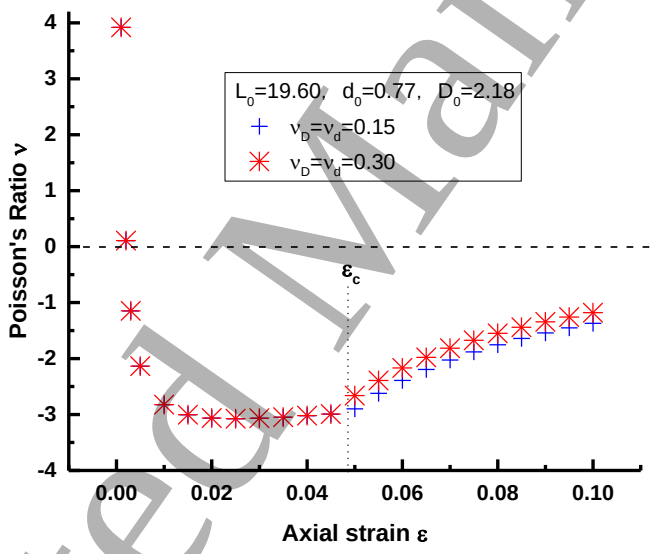

Fig. 9 Effect of Poisson's ratio of soft and stiff yarns on auxetic behavior of APY

The other important parameters which can affect the auxetic behavior of the APY include the diameters of the soft and stiff yarns D_0 and d_0 as well as the pitch length of the APY L_0. To facilitate to investigate their effect, two dimensionless variables R_1 and R_2 are introduced as shown in Eq.51.

$$R_1 = \frac{D_0}{d_0}, \quad R_2 = \frac{L_0}{d_0} \tag{51}$$

The first variable R_1 refers to the diameter ratio of the soft yarn and stiff yarn. Fig. 10a and Fig. 10b show the calculation results when R_1 is changed from 2.00 to 6.00 for two different values of d_0 (0.77 and 0.40), respectively. L_0 is kept unchanged in this case. It can be seen that the auxetic behavior of the APY is decreased with the increase of R_1. This is normal because the auxetic behavior of the APY is achieved when the two stiff yarns are moving towards the center of the APY. The increase of R_1 implicates that diameter of the stiff yarn is relatively decreased as compared with that of the soft yarn, which results in a reduction of the auxetic behavior of the APY. On the other hand, for the same R_1, the auxetic behavior of the APY can be dramatically increased with the increase of d_0 when L_0 is kept unchanged. This can be confirmed by comparing the Poisson's ratio values shown in Fig. 10a and Fig. 10b. The reason is that when L_0 is kept unchanged, the reduction of d_0 means the reduction of yarn helical angle as the small yarn helical angle can produce high auxetic behavior. These results clearly indicate that R_1 cannot affect the auxetic behavior of the APY independently. Hence, to have significant auxetic effect, the diameter of the stiff yarn should be appropriately selected when the soft yarn is given.

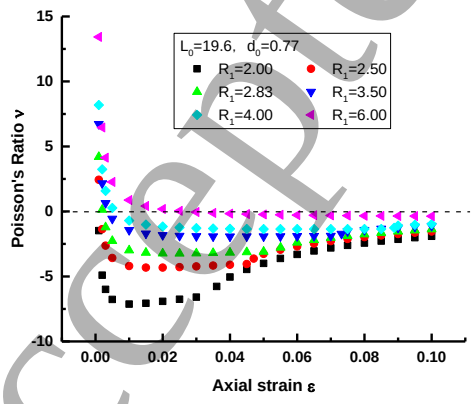

(a)

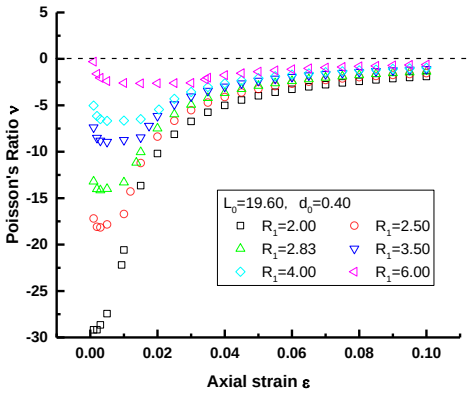

(b)

Fig. 10 Effect of R_1 on auxetic behavior of APY: (a) d_0=0.77; (b) d_0=0.40.

The second variable R_2 refers to the ratio between the pitch length of the APY and the diameter of the stiff yarn. Fig. 11a shows the calculation results when R_1 is changed from 10 to 30 with keeping R_1 constant. It can be seen that the Poisson's ratio of the APY is changed from negative to positive when R_2 is decreased from 30.0 to 10.0. The results indicate that the pitch length of the APY should be large enough or the initial helical angle of the soft yarn should be small to obtain a demonstrable auxetic effect. Fig.11b shows the effect of R_2 on the critical tension strain ε_c. It is found that ε_c is dramatically decreased with the increasing of R_2. This result implicates that the high pitch length of the APY could lead to low extension of the APY, which may reduce its practical application potential.

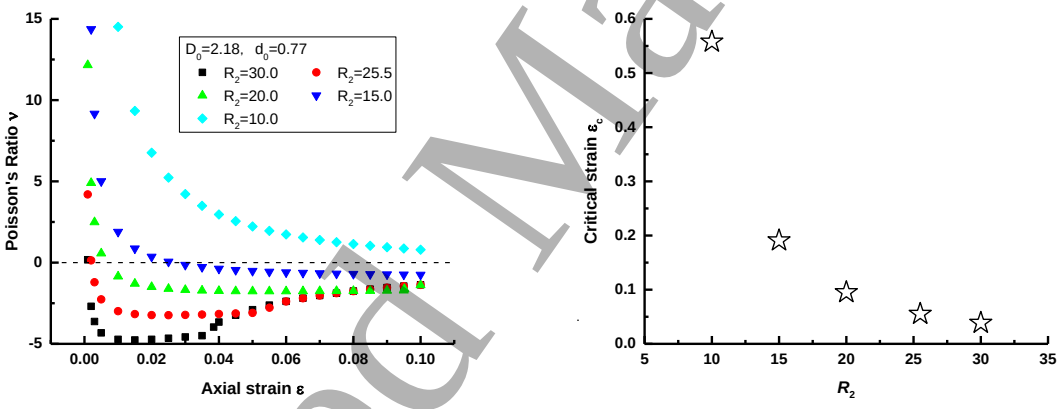

(a) (b)

Fig. 11 Effect of R_2: (a) on auxetic behavior of APY; (b) on critical strain.

Although the effect of R_1 and R_2 on the auxetic behavior of the APY has been discussed separately, the robustness of structural topology has not been studied yet. In this regard, the Poisson's ratio of the APY as a function of axial strain for constant values of R_1 and R_2 (R_1=2.83, R_2=25.50) is drawn in Fig.12. From Fig. 12, it can be seen that the Poisson's ratio values are the same when R_1 and R_2 are kept unchanged even the values of the other

parameters L_0, D_0 and d_2 are different. This result is very useful for the structural design of the APY because its Poisson's ratio is simultaneously controlled by R_1 and R_2. Therefore, the same auxetic behavior can be achieved for APYs fabricated with different soft and stiff yarns, as long as their R_1 and R_2 are kept unchanged.

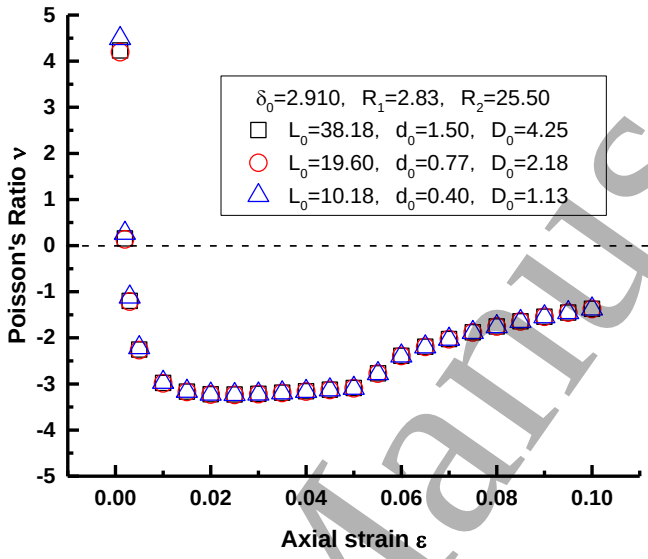

Fig.12 The robustness of structural topology for APY.

5. Conclusions

A theoretical analysis on the deformation behavior of the APY structure was carried out and compared with the experimental results obtained from the previous work. The effects of differential structural parameters were discussed based on the developed tilted angle model. According to the theoretical analysis, the following conclusions can be drawn.

1) The titled angle model developed in this study can correctly predict the variation trend of the auxetic behavior of the APY structure, which first increases and then decreases with the increase of the axial strain. This prediction provides a better understanding of the deformation behavior of the APY under axial extension.

2) The auxetic behavior of the APY are simultaneously controlled by the diameter ratio of the

soft yarn and stiff yarn R_1 as well as the ratio between the pitch length and stiff yarn diameter R_2. The APYs with the same auxetic behavior can be designed and fabricated by using different soft and stiff yarns as long as these two ratios are kept unchanged. The increase of R_1 and decrease of R_2 can increase the auxetic behavior of the APY.

3) The difference in the Poisson's ratio values between the experiment and the theoretical calculations mainly comes from simplified assumptions including the constant diameter and length of the stiff yarn in the initial stage of extension, the ignorance of extrusion and friction among yarn components during the axial extension process, and uniform yarn twist and yarn cross sectional shapes. To get more precise prediction in the Poisson's ratio of the APY, a further analysis based on more realistic assumptions by taking the yarn mechanical properties into consideration is required in the future work.

Acknowledgement

This work was supported by the Research Grants Council of Hong Kong Special Administrative Region Government in the form of a GRF project [grant number 515713].

References

1. Alderson, A. and Alderson, K.L., *Auxetic materials.* Proceedings of the Institution of Mechanical Engineers Part G-Journal of Aerospace Engineering, 2007. **221**(G4): p. 565-575.
2. Lim, T.C., *Longitudinal wave motion in width-constrained auxetic plates.* Smart Materials and Structures, 2016. **25**(5): p. 054008.
3. Allen, T., Shepherd, J., Hewage, T.A.M., Senior, T., Foster, L., and Alderson, A., *Low-kinetic energy impact response of auxetic and conventional open-cell polyurethane foams.* Physica Status Solidi B-Basic Solid State Physics, 2015. **252**(7): p. 1631-1639.
4. Zhou, L., Jiang, L.L., and Hu, H., *Auxetic composites made of 3D textile structure and polyurethane foam.* Physica Status Solidi B-Basic Solid State Physics, 2016. **253**(7): p. 1331-1341.
5. Jiang, L.L. and Hu, H., *Low-velocity impact response of multilayer orthogonal structural composite with auxetic effect.* Composite Structures, 2017. **169**: p. 62-68.
6. Donoghue, J.P., Alderson, K.L., and Evans, K.E., *The fracture toughness of composite laminates with a negative Poisson's ratio.* Physica Status Solidi B-Basic Solid State Physics, 2009. **246**(9): p. 2011-2017.
7. Coenen, V.L. and Alderson, K.L., *Mechanisms of failure in the static indentation resistance of auxetic carbon fibre laminates.* Physica Status Solidi B-Basic Solid State Physics, 2011. **248**(1): p. 66-72.
8. Lakes, R., *FOAM STRUCTURES WITH A NEGATIVE POISSONS RATIO.* Science, 1987. **235**(4792): p. 1038-1040.

9. Lim, T.C., *Auxetic Materials and Structures*. 2015: Springer.

10. Saxena, K.K., Das, R., and Calius, E.P., *Three Decades of Auxetics Research - Materials with Negative Poisson's Ratio: A Review.* Advanced Engineering Materials, 2016. **18**(11): p. 1847-1870.

11. Lakes, R.S., *Negative-Poisson's-Ratio Materials: Auxetic Solids*, in *Annual Review of Materials Research, Vol 47*, D.R. Clarke, Editor. 2017, Annual Reviews: Palo Alto. p. 63-81.

12. Alderson, K.L., Simkins, V.R., Coenen, V.L., Davies, P.J., Alderson, A., and Evans, K.E., *How to make auxetic fibre reinforced composites.* Physica Status Solidi B-Basic Solid State Physics, 2005. **242**(3): p. 509-518.

13. Steffens, F., Rana, S., and Fangueiro, R., *Development of novel auxetic textile structures using high performance fibres.* Materials & Design, 2016. **106**: p. 81-89.

14. Sibal, A. and Rawal, A., *Design strategy for auxetic dual helix yarn systems.* Materials Letters, 2015. **161**: p. 740-742.

15. Lim, T.C., *Semi-auxetic yarns.* Physica Status Solidi B-Basic Solid State Physics, 2014. **251**(2): p. 273-280.

16. Allen, T., Hewage, T., Newton-Mann, C., Wang, W.Z., Duncan, O., and Alderson, A., *Fabrication of Auxetic Foam Sheets for Sports Applications.* Physica Status Solidi B-Basic Solid State Physics, 2017. **254**(12): p. 1700596.

17. Lim, T.C., *Analogies across auxetic models based on deformation mechanism.* Physica Status Solidi-Rapid Research Letters, 2017. **11**(6): p. 1600440.

18. Boldrin, L., Hummel, S., Scarpa, F., Di Maio, D., Lira, C., Ruzzene, M., Remillat, C.D.L., Lim, T.C., Rajasekaran, R., and Patsias, S., *Dynamic behaviour of auxetic gradient composite hexagonal honeycombs.* Composite Structures, 2016. **149**: p. 114-124.

19. McAfee, J. and Faisal, N.H., *Parametric sensitivity analysis to maximise auxetic effect of polymeric fibre based helical yarn.* Composite Structures, 2017. **162**: p. 1-12.

20. Zhang, G.H., Ghita, O., and Evans, K.E., *The fabrication and mechanical properties of a novel 3-component auxetic structure for composites.* Composites Science and Technology, 2015. **117**: p. 257-267.

21. Sloan, M.R., Wright, J.R., and Evans, K.E., *The helical auxetic yarn - A novel structure for composites and textiles; geometry, manufacture and mechanical properties.* Mechanics of Materials, 2011. **43**(9): p. 476-486.

22. Miller, W., Ren, Z., Smith, C.W., and Evans, K.E., *A negative Poisson's ratio carbon fibre composite using a negative Poisson's ratio yarn reinforcement.* Composites Science and Technology, 2012. **72**(7): p. 761-766.

23. Hu, H., Wang, Z.Y., and Liu, S., *Development of auxetic fabrics using flat knitting technology.* Textile Research Journal, 2011. **81**(14): p. 1493-1502.

24. Ge, Z.Y., Hu, H., and Liu, Y.P., *A finite element analysis of a 3D auxetic textile structure for composite reinforcement.* Smart Materials and Structures, 2013. **22**(8): p. 0840058.

25. Ge, Z.Y., Hu, H., and Liu, S.R., *A novel plied yarn structure with negative Poisson's ratio.* Journal of the Textile Institute, 2016. **107**(5): p. 578-588.

26. Ge, Z.Y., Hu, H., and Liu, Y.P., *Numerical analysis of deformation behavior of a 3D textile structure with negative Poisson's ratio under compression.* Textile Research Journal, 2015. **85**(5): p. 548-557.

27. Ge, Z.Y. and Hu, H., *A theoretical analysis of deformation behavior of an innovative 3D auxetic textile structure.* Journal of the Textile Institute, 2015. **106**(1): p. 101-109.

28. Bhattacharya, S., Zhang, G.H., Ghita, O., and Evans, K.E., *The variation in Poisson's ratio caused by interactions between core and wrap in helical composite auxetic yarns.* Composites Science and Technology, 2014. **102**: p. 87-93.

29. Zhang, G.H., Ghita, O.R., and Evans, K.E., *Dynamic thermo-mechanical and impact properties of helical auxetic yarns.* Composites Part B-Engineering, 2016. **99**: p. 494-505.

30. Zhang, G.H., Ghita, O., Lin, C.P., and Evans, K.E., *Varying the performance of helical auxetic yarns by altering component properties and geometry.* Composite Structures, 2016. **140**: p. 369-377.

31. Du, Z.Q., Zhou, M., Liu, H.L., and He, L.G., *Study on negative Poisson's ratio of auxetic yarn under tension: Part 1-Theoretical analysis.* Textile Research Journal, 2015. **85**(5): p. 487-498.

32. Du, Z.Q., Zhou, M., He, L.G., and Liu, H.L., *Study on negative Poisson's ratio of auxetic yarn under tension: Part 2-Experimental verification.* Textile Research Journal, 2015. **85**(7): p. 768-774.

33. Wright, J.R., Sloan, M.R., and Evans, K.E., *Tensile properties of helical auxetic structures: A numerical study.* Journal of Applied Physics, 2010. **108**(4): p. 044905.

34. Ng, W.S. and Hu, H., *Tensile and Deformation Behavior of Auxetic Plied Yarns.* Physica Status Solidi B-Basic Solid State Physics, 2017. **254**(12): p. 1600790.

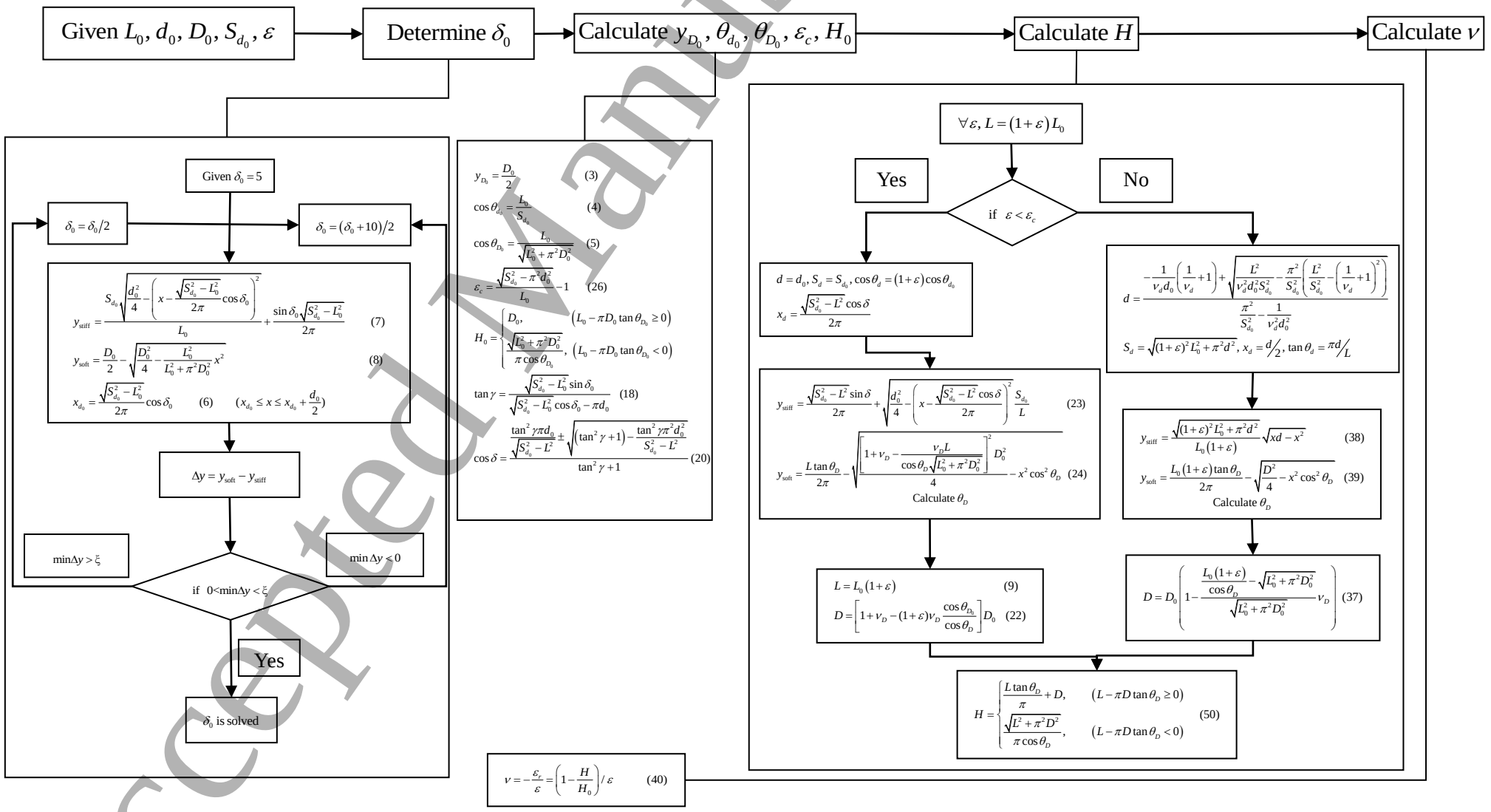

Fig.6 The calculation procedure for the Poisson's ratio of the APY. As the same binary search method for the calculation of δ_0 is used for the calculation of θ_D, for brevity, only the equations for the calculation of y_{soft} and y_{stiff} are listed here. The value of θ_D is ranged from 0 ° to 90 °.